Driving State Adaptive Control of an Active Vehicle Suspension System

Guido Koch and Tobias Kloiber

***Abstract*— A new adaptive vehicle suspension control method is presented that adjusts the controller parametrization to the current driving state and thereby enables to significantly enhance ride comfort while the dynamic wheel load and the suspension deflection remain within safety critical bounds. To this end, the adaptive controller structure dynamically interpolates between differently tuned linear quadratic regulators governed by the dynamic wheel load and the suspension deflection. The stability of the adaptive controller structure is analyzed by means of a common Lyapunov function approach taking into account the nonlinear damper characteristic of the suspension system. In order to provide a realistic framework for the controller design and the performance analysis, a quarter-car test rig based on an all-terrain vehicle suspension that has been equipped with an electrical linear motor to realize an active suspension system, is employed as testbed for the study. On this test rig, the significant performance of the adaptive control concept is successfully validated in a comparison to benchmark suspension controllers.**

***Index Terms*— Active suspension systems, adaptive control, switching control, vehicle dynamics, vehicle suspension control.**

I. Introduction

SUSPENSION systems transfer the forces between the vehicle and the road and thereby mainly determine ride comfort and ride safety. The dynamic behavior of the suspension system significantly influences the handling capabilities of a vehicle, i.e., improvements of the system's performance do not only positively influence the driver's subjective impression of the vehicle but can also lower the number of traffic fatalities by facilitating the driver's authority over the vehicle and preventing physical fatigue of the driver.

Ride comfort and ride safety are governed by the vertical dynamic behavior of the vehicle. If the motions of the four wheels are assumed to be decoupled and the suspension dynamics are only considered in the frequency range of interest for the vertical vehicle dynamics (0–25 Hz), the well-known quarter-car model represents an appropriate modeling framework [1]. It describes the dynamic behavior of the unsprung mass m_w (representing the mass of a tire, the wheel, the brake, the wheel carrier, and parts of the suspension system) and the sprung mass m_c (mainly determined by a quarter of the chassis mass, including passengers and vehicle payload), which are connected by the suspension system. Moreover, a quarter-car model includes a tire model, which is frequently represented by a parallel spring and damper configuration.

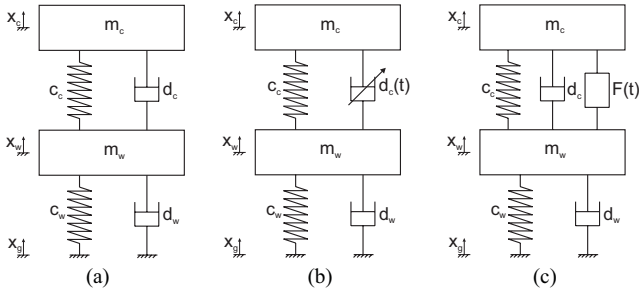

Fig. 1. (a) Passive, (b) semi-active, and (c) fully active suspension system.

Conventional, passive suspension systems include spring and damper elements to isolate the chassis of the vehicle from road-induced vibrations and to prevent the tire from losing ground contact. Mechatronic suspension systems incorporate controlled actuators and thus are able to enhance the performance of the suspension system by modulating the suspension forces [1], [2]. Semi-active suspension systems feature variable dampers, i.e., their damper characteristic can be adjusted within a given range. Due to their low energy consumption, they are available in a wide range of production vehicles [3]. However, the resulting damper forces are restricted by passivity constraints, i.e., they can only counteract the relative motion of the damper. Active suspension systems in contrast require a power supply and are able to generate forces independent of the relative suspension motion. In the case of fully active suspension systems, the actuator bandwidth is higher than 20 Hz. However, due to their energy requirements as well as weight and packaging aspects, fully active suspension systems have not been integrated in production vehicles yet. Fig. 1 depicts the corresponding quarter-car models of the three suspension configurations.

In the following, the equations of motion are derived for the fully active system, including a passive damper, since the other two suspension models result from this model if the control force vanishes, i.e., $F(t) = 0$ (passive system), and the damping is adjustable, i.e., $d_c = d_c(t)$ (semi-active system). For the introductory remarks in this Section, linear component characteristics of the spring and damper elements are assumed. Let

$$\mathbf{x} = \begin{bmatrix} x_1 & x_2 & x_3 & x_4 \end{bmatrix}^T = \begin{bmatrix} x_c - x_w & \dot{x}_c & x_w - x_g & \dot{x}_w \end{bmatrix}^T \quad (1)$$

be the state-vector and $u = F(t)$ and $u_d = \dot{x}_g$ be the control input and the disturbance input of the model, respectively.

Manuscript received December 21, 2011; revised November 16, 2012; accepted December 14, 2012. Manuscript received in final form January 13, 2013. Recommended by Associate Editor S. M. Savaresi.

G. Koch is with the Dynamic Design Laboratory, Stanford University, Stanford, CA 94305 USA (e-mail: guido.koch@googlemail.com).

T. Kloiber is with the Institute of Automatic Control, Technische Universität München, Garching 85748, Germany (e-mail: tobias.kloiber@tum.de).

Color versions of one or more of the figures in this paper are available online at http://ieeexplore.ieee.org.

Digital Object Identifier 10.1109/TCST.2013.2240455

The output vector

$$\mathbf{y} = \begin{bmatrix} \ddot{x}_c & F_{\text{dyn}} & x_c - x_w \end{bmatrix}^T \tag{2}$$

includes the variables of interest for the suspension performance, in particular $F_{\text{dyn}} = c_w(x_g - x_w) + d_w\left(\dot{x}_g - \dot{x}_w\right)$ denoting the dynamic wheel load. The quarter-car model can then be expressed as the linear state-space model

$$\begin{bmatrix} \dot{x}_1 \\ \dot{x}_2 \\ \dot{x}_3 \\ \dot{x}_4 \end{bmatrix} = \begin{bmatrix} 0 & 1 & 0 & -1 \\ -\frac{c_c}{m_c} & -\frac{d_c}{m_c} & 0 & \frac{d_c}{m_c} \\ 0 & 0 & 0 & 1 \\ \frac{c_c}{m_w} & \frac{d_c}{m_w} & -\frac{c_w}{m_w} & -\frac{d_c+d_w}{m_w} \end{bmatrix} \begin{bmatrix} x_1 \\ x_2 \\ x_3 \\ x_4 \end{bmatrix} + \begin{bmatrix} 0 \\ \frac{1}{m_c} \\ 0 \\ -\frac{1}{m_w} \end{bmatrix} u + \begin{bmatrix} 0 \\ 0 \\ -1 \\ \frac{d_w}{m_w} \end{bmatrix} u_d \tag{3}$$

$$\begin{bmatrix} \ddot{x}_c \\ F_{\text{dyn}} \\ x_c - x_w \end{bmatrix} = \begin{bmatrix} -\frac{c_c}{m_c} & -\frac{d_c}{m_c} & 0 & \frac{d_c}{m_c} \\ 0 & 0 & -c_w & -d_w \\ 1 & 0 & 0 & 0 \end{bmatrix} \mathbf{x} + \begin{bmatrix} \frac{1}{m_c} \\ 0 \\ 0 \end{bmatrix} u + \begin{bmatrix} 0 \\ d_w \\ 0 \end{bmatrix} u_d. \tag{4}$$

In the framework of vertical vehicle dynamics, ride comfort is primarily associated with low vertical chassis accelerations $\ddot{x}_c(t)$. However, the human sensitivity for vertical vibrations is especially distinctive in the frequency range 4–8 Hz [4]. Therefore, to assess ride comfort in this paper, the vertical chassis acceleration $\ddot{x}_c(t)$ is weighted using the shaping filter $G_{f,\text{comf}}(s)$ that emphasizes the comfort relevant frequency range [Fig. 2(b)]. To assure ride safety, the dynamic wheel load must be bounded so that longitudinal and lateral forces can be transferred by the tire between the vehicle and the road. However, the objectives ride comfort and ride safety for a suspension system are conflicting. On the one hand, a comfort-oriented suspension should have a low damping of the chassis mass to provide sufficient isolation especially in the frequency range from 4–8 Hz. On the other hand, the resonance peaks of the chassis (sprung mass) and the wheels (unsprung masses) must be limited by sufficiently high damping in order to provide safe driveability and tire road contact for the vehicle. The resulting damping-isolation conflict is visualized in Fig. 2(a) that shows the Bode magnitude plot of the disturbance transfer function $G_{\ddot{x}_c\dot{x}_g}(s)$ for different damping coefficients d_c (see also [2]). The vibration isolation properties of a suspension can be enhanced by softer primary springs. However, packaging requirements limit the available suspension deflection and the resulting deflection bounds need to be taken into account in the suspension design process.

Mechatronic suspension systems can ease the conflict between the objectives ride comfort and ride safety compared to passive suspension systems. Fig. 3 shows this aspect in a conflict diagram. The Pareto front that indicates the achievable performance of passive suspension systems can be shifted toward better ride comfort and safety utilizing active suspension systems. However, a tradeoff between these objectives is still persistent although the tuning parameters change from

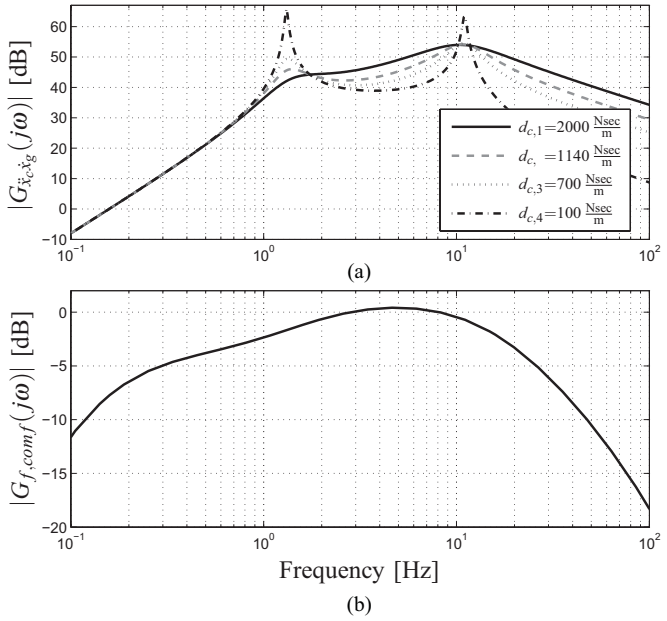

Fig. 2. (a) Damping isolation conflict and (b) Bode magnitude plot of the shaping filter $G_{f,\text{comf}}(s)$ [4].

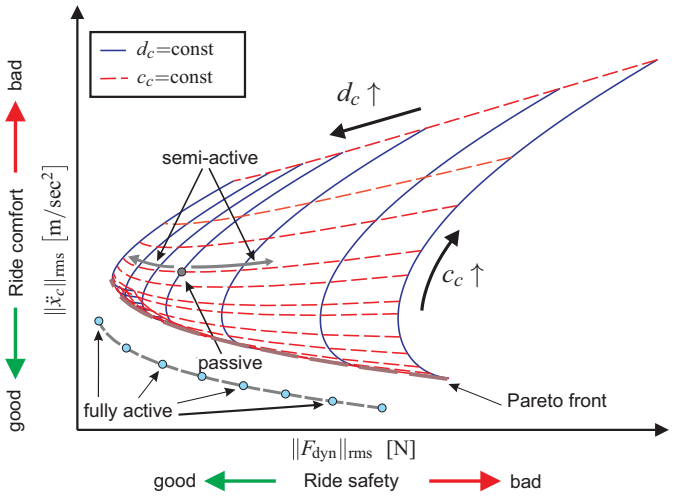

Fig. 3. Conflict diagram for different vehicle suspension configurations.

the choice of passive suspension elements (c_c and d_c) to the choice of the parametrization of the suspension controller.

A wide range of techniques has been presented for suspension controller design. Surveys of suspension control applications, algorithms and performance potentials are e.g., [2], [5], [6]. Moreover, general limitations of mechatronic suspension concepts due to actuator placement restrictions, structural constraints as well as bandwidth and energy limits are discussed, e.g., in [7] and [8]. The scope of control techniques for mechatronic suspension systems reaches from skyhook approaches [9]–[11], controllers utilizing preview information on the road profile ahead of the vehicle [12], [13], optimal control [2], [14], [15], H_∞-control [16], [17], to model predictive control [18], and adaptive control to take into account nonlinear actuator dynamics [19] or unknown or time-varying vehicle parameters [20]–[22].

Already in early works on suspension control (e.g., [5], [23]–[25]) a potential approach to fully utilize the flexibility provided by the integrated actuators has been pointed out: to adaptively adjust controller parameters according to the suspension deflection and/or the dynamic wheel load and to thereby vary the suspension tuning depending on the vehicle's driving state. In [26], Venhovens has proposed an according wheel load adaptive suspension controller that schedules between a comfort focused skyhook damping constant and a ride safety-oriented passive damping configuration. The structure of the adaptation logic utilized in [26] serves as basis for the logic that detects the criticality of the driving state in this paper. In [27], a method adjusting the parametrization of a nonlinear filter depending on the suspension deflection is presented that schedules between different controller settings to prevent exceeding the suspension deflection limits while focusing on ride comfort otherwise. A similar functionality is provided by the linear parameter varying suspension controller presented in [28] and [29]. Lu [30] proposed an estimation scheme for the main frequency components of the road excitation to schedule between mixed H_2/H_∞ multiobjective controllers by means of a simple fuzzy-logic-like scheme. Moreover, approaches have been presented that consider a controller adaptation with respect to tire slip [31] or properties of the road-induced vibration itself [32], [33]. The performance potential of fast adaptive suspension systems, that adjust their dynamic behavior to the driving state of the vehicle or the road profile, has been pointed out in all the previously mentioned works. However, the stability of the adaptive system is seldom discussed in detail, the presented simulations are based on linear suspension models and an experimental validation is not conducted.

This paper presents a control approach to exploit the capability of a mechatronic suspension system by dynamically adjusting the controller parameters with respect to the current driving situation. To this end, an adaptive controller structure is designed, which schedules the controller parametrization according to the current driving state specified in terms of the dynamic wheel load and the suspension deflection. The resulting fast adaptive suspension thus maximizes ride comfort as long as constraints on the dynamic wheel load and the suspension do not tend to be violated. To focus on the improvement resulting from the control concept instead of analyzing limitations from actuator constraints, a fully active suspension configuration is chosen as hardware architecture for this paper.[1] The presented controller design method represents an enhancement of a previous concept of the authors [34] that has been tested in simulations with linear models. Main new approaches addressed in this paper are aspects to be taken into account in the controller design to guarantee stability of the system as well as the experimental performance validation in a realistic framework. For the optimization-based tuning of the linear quadratic regulators (LQRs), a detailed nonlinear quarter vehicle model is utilized. To evaluate the controller performance, the proposed concept is compared to established skyhook-based control strategies as well as a conventional linear quadratic optimal controller. For a more detailed presentation of the results, the reader is referred to [35].

[1]It is noted that the presented techniques can also be applied to slow active or semi-active mechatronic suspension systems.

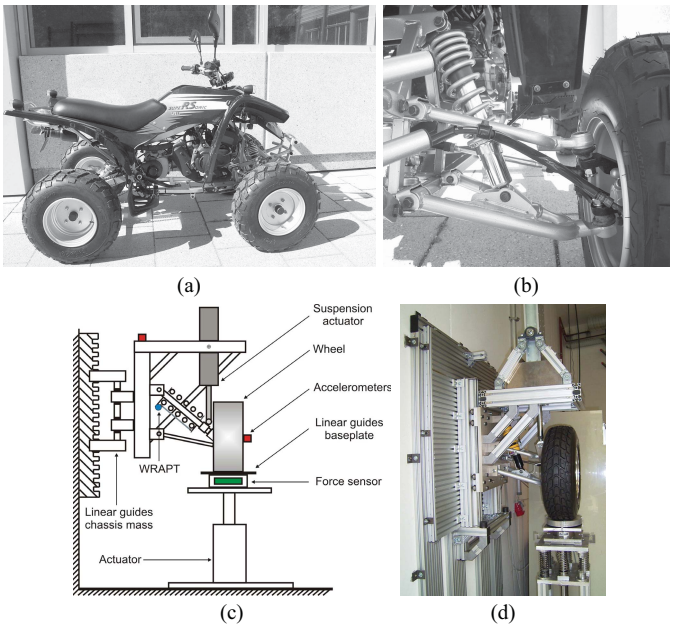

Fig. 4. (a) Experimental vehicle, (b) left front suspension, (c) test rig structure, and (d) test rig.

The remainder of this paper is structured as follows. In Section II, the quarter-car test rig employed for the experimental validation is presented and the requirements for the mechatronic suspension system are formulated in detail. Realistic models of the considered suspension system and the actuator are derived in Section III. Stability aspects, the optimization-based controller parametrization, and an analysis of its performance potential are presented in Section IV. The experimental validation of the controller performance is discussed in a comparison to benchmark systems in Section V.

II. Quarter-Car Test Rig and System Requirements

A. Quarter-Car Test Rig

The test rig is based on an all terrain vehicle (ATV) [Fig. 4(a)] suspension system since this vehicle has a suspension configuration similar to an automobile but it has a considerably lower mass, which simplifies the design of the active suspension system. The left front suspension has been integrated in the test rig structure [Fig. 4(c)] and a force controlled custom-made, ironless, permanently excited synchronous electrical linear motor has been mounted between a vertically guided plate representing the chassis mass and the wheel. A second electrical linear motor is utilized to emulate the road-induced vibrations by exciting the tire vertically. The sensor architecture employed in the active suspension system represents a configuration of modern production vehicles and contains accelerometers for the vertical chassis and wheel acceleration as well as a wire rope actuated position transducer (WRAPT) for the suspension deflection. The current of the

suspension actuator, which is proportional to the actuator force, is also measured. Only these sensors are used for the suspension control and estimation tasks presented in this paper. Additionally, the test rig is equipped with a force sensor to measure the dynamic wheel load for the performance evaluation. A real time controller board operating with a sampling frequency of $f_s = 1$ kHz is used for the controller implementation. More technical details on the test rig are given in [35] and [36].

B. Road Disturbance Input

In general, public roads induce stochastic vibrations to a passing vehicle (see [1] and [2] for more detailed discussions on the properties of road-induced vibrations). In order to provide a realistic framework regarding the excitation signals in this paper, measurements of real road profiles are used for the simulations and for the conducted experiments. The considered road profiles have been recorded by a measurement vehicle equipped with laser scanners on two German country roads. Profile P1 causes large suspension deflections and profile P2 contains primarily high frequency components. Besides stochastic signals also singular disturbance events, such as bumps have a major influence on the ride safety of the vehicle as well as the perception of the driver concerning ride comfort. A simple model of the vertical road displacement $x_g(t)$ resulting from a singular disturbance event is given in [1] as

$$x_g(t) = \begin{cases} h\left(1 - \cos\left(\frac{2\pi v_b}{L} t\right)\right), & \text{for} \quad 0, \leq t \leq \frac{L}{v_b} \\ 0, & \text{else} \end{cases} \tag{5}$$

where h represents half the bump height $\hat{h}$, L is the bump length, and v_b is the velocity of the passing vehicle.

C. System Requirements

The system requirements can be summarized as follows.

1) The root mean square (rms) value of the vertical chassis acceleration $\|\ddot{x}_c\|_{\text{rms}}$ should be minimized to increase ride comfort, especially in the frequency range 4–8 Hz as pointed out in Section I. Thus, $\|\ddot{x}_{c,\text{comf}}\|_{\text{rms}}$ is considered as a measure for ride comfort, which is calculated from $\ddot{x}_c(t)$ after filtering the signal with the shaping filter

$$G_{f,\text{comf}}(s) = \frac{6.9 \cdot 10^4 s^2 (s+6.9)}{(s+0.8)^2 (s+12.6)(s+94.3)(s+628.3)}. \tag{6}$$

This transfer function [see also Fig. 2(b)] is an approximation of the frequency characteristic for the human sensitivity to vertical mechanical vibration given in [37]. Furthermore, $\max(|\ddot{x}_c(t)|)$ is also evaluated to consider peaks in the chassis acceleration signal, which can be especially distinct for singular disturbance events.

2) An important preliminary for ride safety is to ensure contact between the tire and the road. Thus, the transfer of longitudinal and lateral forces is enabled, so that the driver can control the vehicle by steering, throttle, and brake inputs. Therefore, the dynamic wheel load's rms-value should be bounded by

$$\max\left(\|F_{\text{dyn}}\|_{\text{rms}}\right) \leq \frac{(m_c + m_w)g}{3} = \frac{F_{\text{stat}}}{3} \tag{7}$$

where g denotes the gravitational constant and F_{stat} is the static wheel load. This is derived from the 3σ-rule and assures—assuming a normally distributed dynamic wheel load caused by the stochastic disturbance signal—that F_{dyn} remains within $\pm F_{\text{stat}}$ for 99.7% of the time[2] [1]. In the considered test rig application, the static wheel load is $F_{\text{stat}} = 1160.5$ N.

3) The suspension deflection $x_{cw} = x_c - x_w$ at the test rig is limited to ± 0.05 m. Due to the dynamic change of the suspension's equilibrium position caused by the asymmetric damping characteristic when the suspension is subject to road-induced vibrations, the standard deviation $\|x_c - x_w\|_{\text{std}}$ is considered for the analysis of the suspension deflection instead of its rms-value.

4) The displacement Δx_{act} of the suspension actuator is limited to ± 0.05 m, its maximum rms-force is $\max(\|F(t)\|_{\text{rms}}) = 800$ N and its peak force limit is $\max(|F(t)|) = 4$ kN.

5) Minimum power demand of the actuator is intended, which is quantified by the rms-value of the positive mechanical power resulting from the actuator force $F(t)$ and its velocity $v_{\text{act}}(t)$ as

$$\|P^+\|_{\text{rms}} = \sqrt{\frac{1}{T}\int_0^T \left(P^+(\tau)\right)^2 d\tau}$$

with

$$P^+(t) = \begin{cases} F(t)v_{\text{act}}(t), & \text{for } F(t)v_{\text{act}}(t) > 0 \\ 0, & \text{else.} \end{cases} \tag{8}$$

It is noted that for a more realistic analysis of the absolute power demand, the electrical efficiency factors of the actuator system as well as potential recuperation effects have to be taken into account. However, since these factors are not exactly known for the actuator at hand and primarily a relative comparison of power demand between different control concepts is intended, the described approach represents a suitable method for the analysis.

III. Modeling

A. Suspension Component Characteristics and Nonlinearities

1) Suspension Kinematics: The kinematic relations between the deflection of the suspension strut and the vertical movements of the chassis and the wheel are described as proposed in [38] by using a transmission factor $i = \Delta\dot{x}_{el}/\dot{x}_c - \dot{x}_w$ with $\Delta\dot{x}_{el}$ being the relative velocity of the suspension strut in the direction of the element's center line. The factor transforms the forces and kinematic relations at the elements (axial damper force $\bar{F}_d(\Delta\dot{x}_{el})$, axial spring force $\bar{F}_{cc} = \bar{c}_c \Delta x_{el}$ with $\bar{c}_c$ being the spring stiffness) to the corresponding quantities of the quarter-car model (see Fig. 1). According to [38], the primary spring stiffness results as

$$c_c = i^2 \bar{c}_c + \bar{F}_{cc} \frac{di}{d(x_c - x_w)}. \tag{9}$$

[2]Since negative dynamic wheel loads are most critical, the probability that $F_{\text{stat}} - F_{\text{dyn}} > 0$ holds and tire road contact is kept increases to 99.87% due to the symmetry of the Gaussian probability distribution.

TABLE I
PARAMETERS OF THE NONLINEAR QUARTER-CAR MODEL

Model Parameter	Symbol	Value	Unit
Sprung mass	m_c	94.38	[kg]
Unsprung mass	m_w	23.92	[kg]
Primary spring stiffness	$c_c = i^2\bar{c}_c$	8400	[N/m]
Linear tire stiffness	c_w	152186	[N/m]
Friction force spring/damper	$F_{f,1}$	115	[N]
Friction scaling spring/damper	$k_{f,1}$	125	[sec/m]
Friction force chassis mass guides	$F_{f,2}$	20	[N]
Friction scaling chassis mass guides	$k_{f,2}$	125	[sec/m]
Transmission factor	i	0.392	[−]
Tire damping coefficient	d_w	50	[Nsec/m]
Damping ratio sprung mass	D_c	0.39	[−]
Damping ratio unsprung mass	D_w	0.18	[−]
Undamped natural frequency of the sprung mass	f_c	1.5	[Hz]
Undamped natural frequency of the unsprung mass	f_w	12.7	[Hz]

The second term in (9) can be neglected for the considered suspension model because it has been identified to be small (see [36]). Due to the concentric configuration of the suspension strut, the transmission factors for the spring and the damper are the same and the damper force in the coordinates of the quarter-car model results accordingly as $F_d(\dot{x}_{wc}) = i\,\bar{F}_d(i\dot{x}_{wc})$ with $\dot{x}_{wc} = \dot{x}_w - \dot{x}_c$. The parameters are given in Table I.

2) Suspension Component Characteristics: The main nonlinearity of the suspension system is the degressive force-velocity characteristic of the damper. The characteristic has been supplied by the manufacturer of the damper and is depicted in Fig. 5(a). The characteristic of the primary spring has been identified to be linear in the operating range of the test rig, i.e., the spring force is calculated as $F_c = c_c(x_c - x_w)$. The nonlinearity resulting from the spring's end stop is not taken into account since the adaptive controller presented in Section IV prevents the suspension deflection from exceeding its limits. The tire force-deflection characteristic has been identified to be progressive [Fig. 5(b)] but can be linearized in the operating point given by the static wheel load. The identified tire damping is comparably small ($d_w = 50$ Nsec/m), which is coherent with the literature (see [1]).

3) Friction Effects: Coulomb friction forces (see [39]) in the suspension ($F_{f,1}$) and in the vertical guides of the chassis mass ($F_{f,2}$) are taken into account for the modeling. They are approximated by tanh-functions for smooth zero crossings (see [40]) so that the resulting friction model is $F_{f,i} = \hat{F}_{f,i}\tanh(\Delta v_i k_{f,i})$ with $\Delta v_1 = \dot{x}_c$, $\Delta v_2 = \dot{x}_c - \dot{x}_w$ and the scaling factors $k_{f,1} = k_{f,2}$. The numerical values have been identified experimentally (see Table I and [36]).

B. Actuator Model

The input signal of the suspension actuator is a control voltage $u_v(t)$ and the measured output signal is the actuator current $i_{\text{act}}(t)$. Identification experiments have indicated that the dynamic behavior of the actuator current can be modeled using a first order low pass and a time delay of $T_d = 4$ msec,

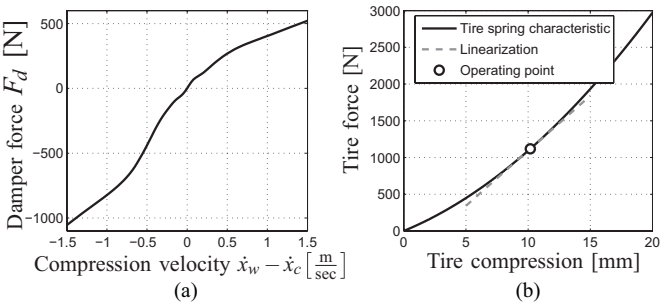

Fig. 5. Nonlinear characteristics of the damper in coordinates of (a) quarter-car model and (b) tire.

which is considered using a first order Padé-approximation for the corresponding transfer function $e^{-T_d s} \approx (T_d s + 1)^{-1}$ (see [41]). The resulting second-order actuator model is

$$\dot{\mathbf{x}}_{lm}(t) = \underbrace{\begin{bmatrix} -320.4019 & 0 \\ 250 & -250 \end{bmatrix}}_{\mathbf{A}_{lm}} \mathbf{x}_{lm}(t) + \underbrace{\begin{bmatrix} 1.2131 \\ 0 \end{bmatrix}}_{\mathbf{b}_{lm}} u_v(t) \quad (10)$$

$$i_{\text{act}}(t) = \underbrace{\begin{bmatrix} 0 & 839.4076 \end{bmatrix}}_{\mathbf{c}_{lm}^T} \mathbf{x}_{lm}(t) \quad (11)$$

with $\mathbf{x}_{lm}(t)$ being the actuator state vector. The measured actuator current $i_{\text{act}}(t)$ is proportional to the actuator force ($1\,\text{A} \sim 0.1\,\text{kN}$). The actuator bandwidth is approx. $\omega_{\text{act}} = 2\pi \cdot 28.6\,\frac{\text{rad}}{\text{sec}}$, which is sufficient for the fully active suspension system.

C. Nonlinear Suspension Model

The resulting test rig model includes the actuator dynamics and the nonlinear quarter-car model of the suspension system. The input signals are the vertical velocity of the road excitation $u_d = \dot{x}_g(t)$ and the actuator control input $u_v(t)$. The resulting suspension model has the order six and can be formulated with the state vector

$$\mathbf{x} = \begin{bmatrix} x_c - x_w & \dot{x}_c & x_w - x_g & \dot{x}_w & x_{lm,1} & x_{lm,2} \end{bmatrix}^T \quad (12)$$

and the output vector $\mathbf{y}_m = \begin{bmatrix} \ddot{x}_c & \ddot{x}_w & x_c - x_w \end{bmatrix}^T$ that gathers the measurement signals, which can be employed for suspension control. The nonlinear state-space model is expressed as

$$\dot{\mathbf{x}}(t) = \mathbf{f}(\mathbf{x}(t), u_v(t), u_d(t)) \quad (13)$$

$$\mathbf{y}_m(t) = \mathbf{h}(\mathbf{x}(t), u_v(t), u_d(t)). \quad (14)$$

The performance output vector, which contains the relevant system quantities according to the requirements formulated in Section II-C, is defined as

$$\mathbf{y}(t) = \begin{bmatrix} \ddot{x}_c & F_{\text{dyn}} & x_c - x_w \end{bmatrix}^T \quad (15)$$

and can be expressed by reformulating (14) as $\mathbf{y}(t) = \tilde{\mathbf{h}}(\mathbf{x}(t), u_v(t), u_d(t))$. The explicit model formulation is omitted for the sake of brevity but is given in similar form in [35] and [36]. The natural frequencies of the sprung and the unsprung mass are $f_c = 1.5\,\text{Hz}$ and $f_w = 12.7\,\text{Hz}$ and the damping ratio of the sprung mass is $D_c \approx 0.39$. Thus, the suspension has a similar vertical dynamic behavior to an automotive suspension system (compare e.g., [1]).

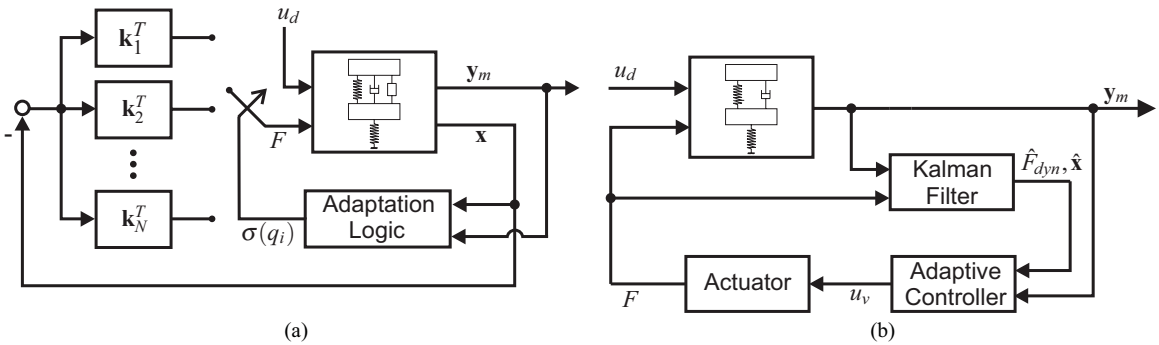

Fig. 6. (a) Adaptive controller structure and (b) realization of the approach at the test rig.

IV. Controller Design

As pointed out in Section I, the main idea of the following driving state adaptive suspension control approach is to focus on ride comfort as long as the limits for the dynamic wheel load and suspension deflection permit. Only if the driving state tends to become critical, a more safety-oriented controller parametrization is chosen. To this end, an adaptive controller structure is proposed, which is shown in Fig. 6. An adaptation logic schedules between N differently tuned state feedback controllers $\mathbf{k}_i^T$ depending on the dynamic wheel load and the suspension deflection. In Section IV-C, it is derived that $N = 3$ represents a good tradeoff between controller performance and complexity of the controller design and implementation. The term $\sigma(q_i)$ denotes a scheduling signal depending on the scheduling parameters $q_{\text{fdyn}}(t)$ and $q_{\text{susp}}(t)$, which reflect the criticality of the vertical dynamic driving state of the vehicle (see Section IV-A).

Since the system requirements for ride safety and ride comfort involve rms-formulations, LQRs are chosen to be implemented in the adaptive controller structure. They minimize a quadratic cost functional and have a fairly transparent tuning procedure using weighting matrices for the performance output signals and the control input. LQR designs are frequently employed in the literature for performance potential studies of suspension systems (see [2], [5], [25], [42]). For the parametrization of the state feedback controllers in this paper, an optimization-based procedure is utilized (see Section IV-C).

In order to prevent discontinuities in the control signal caused by discontinuous switching between the controllers, an interpolation approach that provides continuous scheduling of the controller gains is realized. The corresponding control law is

$$u(t) = -\mathbf{k}_{\text{adp}}^T(t)\mathbf{x}(t) \tag{16}$$

$$\mathbf{k}_{\text{adp}}^T(t) = (1 - q_{\text{susp}}(t)) \Big((1 - q_{\text{fdyn}}(t))\mathbf{k}_{\text{comf}}^T + \ldots + q_{\text{fdyn}}(t)\mathbf{k}_{\text{safe}}^T \Big) + q_{\text{susp}}(t)\mathbf{k}_{\text{susp}}^T \tag{17}$$

with $\mathbf{k}_{\text{comf}}^T$, $\mathbf{k}_{\text{safe}}^T$, and $\mathbf{k}_{\text{susp}}^T$ being state feedback gain vectors for the objectives ride comfort enhancement, dynamic wheel load minimization, and suspension deflection minimization, respectively. The design of these state feedback controllers and an analysis of the performance potential resulting from the scheduling approach are presented in Sections IV-C and IV-D.

For the implementation of the state feedback based controller structure [see Fig. 6(b)], an estimator concept is required since not all state variables are measured and for the calculation of the scheduling parameter $q_{\text{fdyn}}(t)$ knowledge of the dynamic wheel load $F_{\text{dyn}}(t)$ is required. The employed estimator concept involves two parallel Kalman filters to infer estimates of the state vector of the vehicle suspension system defined in (1) and has been presented by the authors in [43]. The estimator takes into account the nonlinear damper characteristic by considering the damper force, that is calculated from the estimated damper velocity and the known damper characteristic, as an additional input signal for the Kalman filters (an approach proposed in [44]). In order to establish a good estimation performance despite the nonlinearities of the system, the two parallel Kalman filters have been parametrized by means of genetic optimization. Each of them supplies the required state variables (1), that are estimated with maximum quality, and an estimate for the dynamic wheel load $\hat{F}_{\text{dyn}}$ is also provided. In [45], it has been experimentally shown that the estimator concept outperforms an Extended Kalman filter for the considered suspension control application.

A. Adaptation Logic

The task of the adaptation logic is to detect the criticality of the driving state from the measured and estimated data. To this end, the two scheduling parameters $q_{\text{fdyn}}(t)$ and $q_{\text{susp}}(t)$ are determined by a method that extends an approach proposed by Venhovens in [26].

1) Wheel Load Adaptation: The scheduling parameter $q_{\text{fdyn}}(t)$ is derived from the estimate of the dynamic wheel load $\hat{F}_{\text{dyn}}(t)$ and takes into account slow variations of the dynamic wheel load, i.e., changes of its rms-value, as well as rapid increases. While the latter is realized by the upper branch (fast adaptation) in the block diagram shown in Fig. 7, the variance of the dynamic wheel load is approximated by the slow adaptation part (lower branch).

For the fast adaptation, a nonlinear scaling function $w(\hat{F}_{\text{dyn}}/F_{\text{stat}})$ [Fig. 8(a)], which is constructed from a fourth-order polynomial and a dead zone, causes $e_f(t)$ to rise if $|\hat{F}_{\text{dyn}}|/F_{\text{stat}} \geq \Gamma_{\text{fdyn,f}} = 0.8$ holds (see also [27] for a similar scheduling approach). For the calculation of the fast adaptation

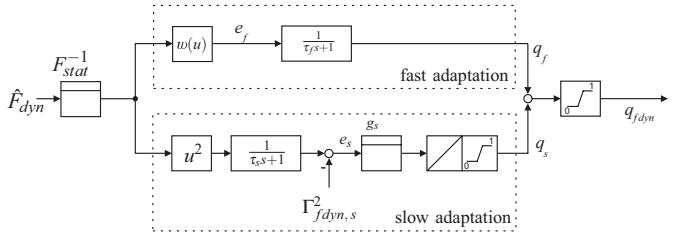

Fig. 7. Wheel load adaptation structure.

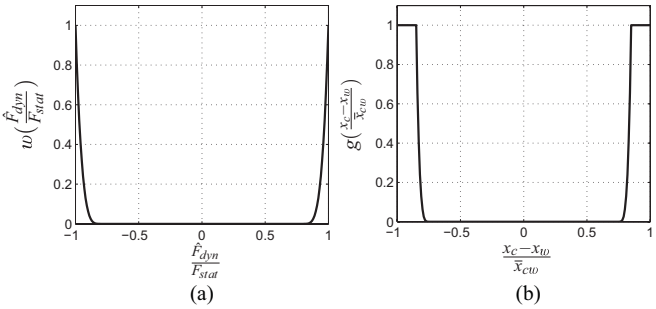

Fig. 8. (a) Nonlinear scaling functions $w(\frac{\hat{F}_{\text{dyn}}}{F_{\text{stat}}})$ for the fast dynamic wheel load adaptation and (b) $g(\frac{x_c-x_w}{\bar{x}_{cw}})$ for the fast suspension deflection adaptation.

signal $q_f(t)$, a low-pass filter with a time constant $\tau_f = 1/2\sqrt{m_w/(c_c+c_w)} \approx 0.006$ sec is employed to avoid too rapid changes in the adaptation of the controller parameters.

The lower branch illustrated in Fig. 7 calculates the slow adaptation signal $q_s(t)$ to take into account slow changes of the stochastic properties of the road excitation. Following Venhovens' approach in [26], the variance of the estimated dynamic wheel load is approximated by

$$\sigma^2_{\hat{F}_{\text{dyn}}}(s) \approx \frac{1}{\tau_s s+1}\hat{F}^2_{\text{dyn}}(s). \tag{18}$$

The time constant of the low-pass filter τ_s is chosen as $\tau_s = 1/2\sqrt{m_c/c_c} \approx 0.053$ sec. The ratio of the dynamic wheel load filtered in this manner and the static wheel load is compared to the bound $\Gamma_{\text{fdyn,s}} = \frac{1}{3}$ according to the 3σ-rule-based system requirement formulated in (7). The deviation $e_s(t)$ is integrated by an output-limited integrator with an output signal range of $[0, 1]$ resulting in $q_s(t)$. It is noted that output limitation in this context refers to deactivation of the integral action when the limit is reached to prevent wind-up. For the dynamic wheel load adaptation, the integrator gain is $g_s = 1$. The resulting scheduling parameter is $q_{\text{fdyn}}(t) = \min\big(1, q_s(t) + q_f(t)\big)$. While $q_{\text{fdyn}}(t)$ remains close to zero, a comfort-oriented controller can be activated [see (17)]. Accordingly, if $q_{\text{fdyn}}(t)$ rises, it indicates higher dynamic wheel loads and the urgency to activate a more safety-oriented controller parametrization. The main differences compared to Venhovens approach in [26] for the wheel load adaptation logic are the output-limiting of the integrator instead of the reset approach presented in [26], smaller time constants τ_f and τ_s to improve the response time of the logic, and a higher gain value for g_s to ensure ride safety by the logic.

2) Suspension Deflection Adaptation: For the calculation of the scheduling signal $q_{\text{susp}}(t)$, which indicates if the suspension deflection becomes critical, the same structure of the adaptation logic as for the dynamic wheel load (see Fig. 7) is employed. As in the dynamic wheel load adaptation scheme, the slow adaptation is based on an rms-constraint $\max\left(\|x_{cw}\|_{\text{rms}}\right) \leq \bar{x}_{cw}/3$ derived from the 3σ-rule (with $\bar{x}_{cw} = 5$ cm). In the fast adaptation, the nonlinear scaling function $g(x_{cw}/\overline{x}_{cw})$ [Fig. 8(b)], that is substituted for $w(u)$ in Fig. 7, is also constructed from a dead zone and a fourth-order polynomial. The time constant of the low-pass filter in the fast adaptation is chosen as $\tau_{f,\text{susp}} = 1/3\sqrt{m_w/(c_c+c_w)} \approx 0.004$ sec to be able to quickly prevent the suspension from hitting the limits. The parameters of the slow adaptation are chosen as $\tau_{\text{s,susp}} = \sqrt{m_c/c_c} \approx 0.110$ sec and $g_{\text{s,susp}} = 1.5$.

B. Preliminaries for Stability of the Switched System

In order to guarantee stability for the proposed adaptive controller structure (Fig. 6), two main aspects have to be taken into account, both of which are addressed in the following.

1) For the design of the LQRs, a linear suspension model must be employed although the dynamic behavior of the physical system is nonlinear. If the nonlinear damper characteristic is linearized at its origin (at the equilibrium, the damper velocity is zero), the damper forces in the linearized model are higher than the ones in the nonlinear system due to the degressive shape of the damper characteristic. Consequently, applying the resulting LQR to the original system could cause instability, which must be prevented by altering the linear model employed for the LQR design.
2) The state feedback controller gains of the closed-loop system can change rapidly due to the adaptation to the current driving state. Therefore, the stability of the adaptive system with the scheduling control approach (17) must be analyzed.

a) Nonlinear damper characteristic: For the following analysis, the degressive force-velocity characteristic of the damper is considered to be the only nonlinearity of an otherwise linear quarter-car model obtained from linearizing the tire force-deflection characteristic [see Fig. 5(b)] and omitting the friction forces. If the state-dependent damper coefficient $d_c(\mathbf{x}) = d_c(\dot{x}_{wc}) = F_d(\dot{x}_{wc})/\dot{x}_{wc}$ with $\dot{x}_{wc} = \dot{x}_w - \dot{x}_c$ is introduced, the system can be represented in quasi-linear form as

$$\dot{\mathbf{x}} = \underbrace{\begin{bmatrix} 0 & 1 & 0 & -1 \\ -\frac{c_c}{m_c} & -\frac{d_c(\mathbf{x})}{m_c} & 0 & \frac{d_c(\mathbf{x})}{m_c} \\ 0 & 0 & 0 & 1 \\ \frac{c_c}{m_w} & \frac{d_c(\mathbf{x})}{m_w} & -\frac{c_w}{m_w} & -\frac{d_c(\mathbf{x})+d_w}{m_w} \end{bmatrix}}_{\mathbf{A}(\mathbf{x})} \mathbf{x} + \underbrace{\begin{bmatrix} 0 \\ \frac{1}{m_c} \\ 0 \\ -\frac{1}{m_w} \end{bmatrix}}_{\mathbf{b}} u. \tag{19}$$

In order to obtain a linear system for the controller design $d_c(\mathbf{x})$ in (19) is replaced by its minimum value $d_{c,\min}$ on the damper velocity interval $\dot{x}_{cw} \in [-1.5$ m/sec, 1.5 m/sec$]$ (see Fig. 9). This interval represents a conservative approximation of realistic relative damper velocities based on the insights from simulations and measurements (see also [46]).

It is intended to show that (19) is asymptotically stable with a state feedback controller that has been designed to asymp-

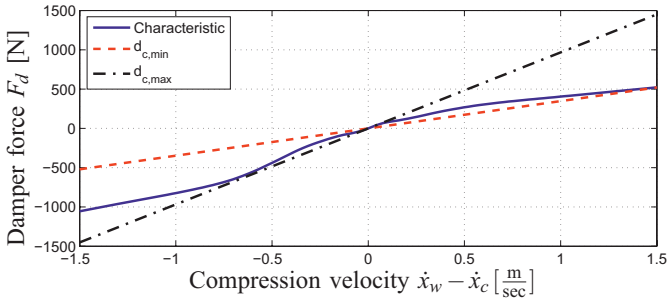

Fig. 9. Damper characteristic (in coordinates of the quarter-car model) and different linear approximations.

totically stabilize the linear system with minimum damping. This is done by means of the circle criterion.

To this end, (19) with $u = -\mathbf{k}^T\mathbf{x}$ must be transformed into a feedback connection of a linear dynamical system and a nonlinear element (the damper characteristic). This is achieved by defining the output signal $y = x_4 - x_2$ and the nonlinearity $\Psi(y) = F_d(y) - d_{c,\min} y$. Then the closed-loop system can be represented in the desired form

$$\dot{\mathbf{x}} = \underbrace{\begin{bmatrix} 0 & 1 & 0 & -1 \\ -\frac{c_c}{m_c} & -\frac{d_{c,\min}}{m_c} & 0 & \frac{d_{c,\min}}{m_c} \\ 0 & 0 & 0 & 1 \\ \frac{c_c}{m_w} & \frac{d_{c,\min}}{m_w} & -\frac{c_w}{m_w} & -\frac{d_{c,\min}+d_w}{m_w} \end{bmatrix}}_{\mathbf{A}_{\text{lin}}(d_{c,\min})\mathbf{x} - \mathbf{b}\mathbf{k}^T\mathbf{x} = \mathbf{A}_{\text{reg}}\mathbf{x}} \mathbf{x} - \mathbf{b}\mathbf{k}^T\mathbf{x} - \underbrace{\begin{bmatrix} 0 \\ -\frac{1}{m_c} \\ 0 \\ \frac{1}{m_w} \end{bmatrix}}_{\mathbf{b}_{F_d}} \Psi(y) \tag{20}$$

$$y = \underbrace{\begin{bmatrix} 0 & -1 & 0 & 1 \end{bmatrix}}_{\mathbf{c}^T} \mathbf{x} \tag{21}$$

with $(\mathbf{A}_{\text{reg}}, \mathbf{b}_{F_d})$ being controllable and $(\mathbf{A}_{\text{reg}}, \mathbf{c}^T)$ being observable, respectively. From the shape of the nonlinear damper characteristic (Fig. 9), it becomes obvious that $\Psi(y)$ satisfies the sector condition

$$0 \le y\Psi(y) \le y^2 \left(d_{c,\max} - d_{c,\min}\right) \quad \forall\, y \in \left[-1.5\frac{\text{m}}{\text{sec}}, 1.5\frac{\text{m}}{\text{sec}}\right]. \tag{22}$$

The transfer function of the linear system is given by $G(s) = \mathbf{c}^T(s\mathbf{I} - \mathbf{A}_{\text{reg}})^{-1}\mathbf{b}_{F_d}$, which is Hurwitz since $u = -\mathbf{k}^T\mathbf{x}$ asymptotically stabilizes the linear system with minimum damping $d_{c,\min}$. Hence, it follows that (20) is absolutely stable for all nonlinearities satisfying (22) if

$$\text{Re}[G(j\omega)] > -\frac{1}{d_{c,\max} - d_{c,\min}} \tag{23}$$

holds [47, Th. 10.1].

The LQRs are designed for the linear system representation with minimum damping and the circle criterion (23) is tested in the controller design process numerically for every controller presented in Section IV-C. If (23) holds, it is concluded that the respective closed-loop system is asymptotically stable in the relevant operating range despite the nonlinear damper characteristic.

b) Common quadratic Lyapunov function approach: In the following, a common quadratic Lyapunov function (CQLF) approach is used to establish asymptotic stability of the unperturbed adaptively controlled system [Fig. 6(a) with $u_d(t) = 0$] taking into account the nonlinear damper characteristic.

Proposition 1: Consider (19) with $u = -\mathbf{k}_{\text{adp}}^T\mathbf{x}$, where $\mathbf{k}_{\text{adp}}^T$ is defined in (17). Assume there is a matrix $\mathbf{P} = \mathbf{P}^T > 0$ and an $\epsilon > 0$ such that

$$\mathbf{P}\mathbf{A}^{(i)} + \left(\mathbf{A}^{(i)}\right)^T \mathbf{P} \le -\epsilon\mathbf{I} \tag{24}$$

with $\mathbf{I}$ representing the unity matrix of appropriate dimension, holds for all matrices

$$\mathbf{A}^{(1)} = \mathbf{A}_{\text{lin}}(d_{c,\min}) - \mathbf{b}\mathbf{k}_{\text{comf}}^T, \quad \mathbf{A}^{(2)} = \mathbf{A}_{\text{lin}}(d_{c,\max}) - \mathbf{b}\mathbf{k}_{\text{comf}}^T \tag{25}$$

$$\mathbf{A}^{(3)} = \mathbf{A}_{\text{lin}}(d_{c,\min}) - \mathbf{b}\mathbf{k}_{\text{safe}}^T, \quad \mathbf{A}^{(4)} = \mathbf{A}_{\text{lin}}(d_{c,\max}) - \mathbf{b}\mathbf{k}_{\text{safe}}^T \tag{26}$$

$$\mathbf{A}^{(5)} = \mathbf{A}_{\text{lin}}(d_{c,\min}) - \mathbf{b}\mathbf{k}_{\text{susp}}^T, \quad \mathbf{A}^{(6)} = \mathbf{A}_{\text{lin}}(d_{c,\max}) - \mathbf{b}\mathbf{k}_{\text{susp}}^T \tag{27}$$

with $\mathbf{A}_{\text{lin}}(d_{c,\max})$ following from (19) accordingly. Then, (19) is uniformly exponentially stable for arbitrary $q_{\text{susp}}(t)$: $[0,\infty) \to [0,1]$ and $q_{\text{fdyn}}(t) : [0,\infty) \to [0,1]$ and $d_{c,\min} \le d_c \le d_{c,\max}$.

Proof: Following the derivation of [47, Th. 10.4], for a given trajectory $\mathbf{x}(t)$ the time-varying gain $r(t)$ defined by $\Psi(y) = r(t)\,(x_4(t) - x_2(t))$ is introduced. By assumption $0 \le r(t) \le d_{c,\max} - d_{c,\min}$ holds irrespective of the particular trajectory. Utilizing $r(t)$ and the system representation (20), the time derivative of the Lyapunov function candidate $V(\mathbf{x}) = \mathbf{x}^T\mathbf{P}\mathbf{x}$ can be formulated as

$$\dot{V}(\mathbf{x},t) = \mathbf{x}^T\left(\mathbf{P}\tilde{\mathbf{A}} + \tilde{\mathbf{A}}^T\mathbf{P}\right)\mathbf{x} =: W(\mathbf{x}, q_{\text{susp}}(t), r(t), q_{\text{fdyn}}(t)) \tag{28}$$

with

$$\tilde{\mathbf{A}}(q_{\text{susp}}(t), r(t), q_{\text{fdyn}}(t)) = \mathbf{A}_{\text{lin}}(d_{c,\min}) - \mathbf{b}\mathbf{k}_{\text{adp}}^T - \mathbf{b}_{F_d} r(t)\mathbf{c}^T. \tag{29}$$

Due to the structure of $\mathbf{k}_{\text{adp}}^T$ defined in (17), $W(\mathbf{x}, q_{\text{susp}}(t), r(t), q_{\text{fdyn}}(t))$ is a multilinear function in $q_{\text{susp}}(t)$, $r(t)$ and $q_{\text{fdyn}}(t)$ over the convex hypercube

$$H = \left\{ \begin{bmatrix} q_{\text{susp}} \\ r \\ q_{\text{fdyn}} \end{bmatrix} \middle| \begin{bmatrix} 0 \\ 0 \\ 0 \end{bmatrix} \le \begin{bmatrix} q_{\text{susp}} \\ r \\ q_{\text{fdyn}} \end{bmatrix} \le \begin{bmatrix} 1 \\ d_{c,\max} - d_{c,\min} \\ 1 \end{bmatrix} \right\} \tag{30}$$

where the inequality is to be interpreted componentwise. Moreover, if q_{susp} and r are subsumed in $\mathbf{z} = [\, q_{\text{susp}}\ r\,]^T$, from (17) it follows that $W(\mathbf{x}, \mathbf{z}, q_{\text{fdyn}})$ is affine in $\mathbf{z}$ for a fixed q_{fdyn}, and it is also affine in q_{fdyn} for a fixed $\mathbf{z}$. Thus, $W(\mathbf{x}, \mathbf{z}, q_{\text{fdyn}})$ is biaffine and hence biconvex in $\mathbf{z}$ and q_{fdyn}. Therefore, by [48, Lemma 1], it attains its maximum value over H at one of the vertices of H. Consequently, it suffices

to prove that $W(\mathbf{x}, \mathbf{z}, q_{\text{fdyn}}) \leq -\epsilon \mathbf{x}^T \mathbf{x}$ holds at the vertices of H to ensure that $W(\mathbf{x}, \mathbf{z}, q_{\text{fdyn}}) \leq -\epsilon \mathbf{x}^T \mathbf{x}$ is satisfied for all $[\, q_{\text{susp}} \; r \; q_{\text{fdyn}} \,]^T \in H$. If the latter holds, it follows that $\dot{V}(\mathbf{x}, t) \leq -\epsilon \mathbf{x}^T \mathbf{x}$ is satisfied along the trajectories of the adaptively controlled system. This proves uniform exponential stability. ■

After a set of controllers $\mathbf{k}_{\text{comf}}^T$, $\mathbf{k}_{\text{safe}}^T$, $\mathbf{k}_{\text{susp}}^T$ has been determined, the YALMIP optimization toolbox (see [49]) and the SeDuMi solver (see [50]) for MATLAB can be used to test if a matrix $\mathbf{P}$ satisfying the conditions given in Proposition 1 (with $\epsilon = 1$) can be calculated numerically.

It is noted that in general, the system state will not tend to the origin for $t \to \infty$ due to the stochastic and persistent nature of the road-induced disturbance $\dot{x}_g(t)$. However, since the system is uniformly exponentially stable it is also totally stable (see [51]) and thus stability is preserved despite small disturbances, i.e., those caused by realistic road excitations $\dot{x}_g$. For a more detailed discussion on this matter, the reader is referred to [35].

C. Optimization-Based LQR Design

The parametrization of the LQR-based state feedback controllers is done by means of numerical optimization taking into account the stability considerations described in the previous Section. The LQR design is conducted for the linear model[3] resulting from (19) with $d_c(\mathbf{x}) = d_{c,\min}$. The actuator dynamics are not considered for the LQR-design since the actuator bandwidth (28.6 Hz) is above the frequency range of interest in suspension control (0–25 Hz, see [1]). However, it is noted that the optimization-based parametrization of the controller gains $\mathbf{k}_i^T \in \mathbb{R}^{1\times 4}$ is accomplished utilizing simulations of the sixth-order model, including the actuator dynamics and all nonlinearities of the system presented in Section III.

With the control input being the actuator force $u(t) = F(t)$ and the performance output $\mathbf{y}(t)$ as defined in (15), the performance index for the LQR design is chosen as

$$J_{LQR} = \int_0^\infty \left(\mathbf{y}^T \mathbf{Q}_y \mathbf{y} + R u^2 \right) dt \tag{31}$$

where R is fixed[4] at $R = 1$ and $\mathbf{Q}_y = \text{diag}\left(\left[\, q_{\ddot{x}_c} \; q_{F_{\text{dyn}}} \; q_{x_{cw}} \,\right] \right)$ is positive definite. Consequently, the decision variables for the numerical optimization are the diagonal entries of $\mathbf{Q}_y$, which are subsumed in the vector

$$\eta = \left[\, q_{\ddot{x}_c} \; q_{F_{\text{dyn}}} \; q_{x_{cw}} \,\right]^T \tag{32}$$

and the vectorial cost functional is chosen according to the control objectives as

$$\mathbf{J}_t(\eta) = \left[\, \|\ddot{x}_{c,\text{comf}}\|_{\text{rms}} \;\; \|F_{\text{dyn}}\|_{\text{rms}} \,\right]^T. \tag{33}$$

The resulting multiobjective optimization problem for the determination of Pareto optimal controller weights can be formulated as

$$\min \;\; \mathbf{J}_t(\eta) \tag{34}$$

$$\text{s.t.} \;\; \max_{t\in[0,T_{\text{sim}}]} \left(|x_{cw}(t)| \right) \leq 0.05\,\text{m} \tag{35}$$

where T_{sim} denotes the simulation time. By (35), the suspension deflection limits are taken into account. For the optimization, the measured data of road profile P1 is used (passed with the velocity $v_{p1} = 50$ km/h) because it represents a typical broadband stochastic road profile. The optimization problem (34) and (35) is solved by means of the multiobjective genetic algorithm NSGA-II (see [52]). The parameter space for η is discretized logarithmically due to the large specified range for the decision variables, and 200 individuals and 35 generations are chosen for the optimization. A similar optimization approach has been presented in [53] for the design of H_∞-controllers.

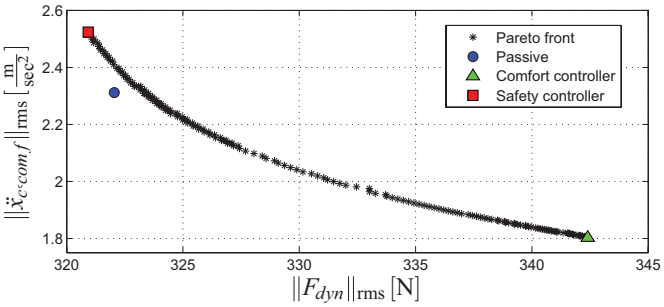

Fig. 10. Pareto front for comfort and safety-oriented LQR parametrizations.

The resulting Pareto front has a gap over an interval of $\|F_{\text{dyn}}\|_{\text{rms}}$, in which no Pareto-optimal configurations exist. Fig. 10 depicts the part of the Pareto front that is relevant for suspension control, i.e., the part with low chassis accelerations $\|\ddot{x}_{c,\text{comf}}\|_{\text{rms}}$. From the end-points of this part of the Pareto front, the comfort controller $\mathbf{k}_{\text{comf}}^T$ and the safety controller $\mathbf{k}_{\text{safe}}^T$ are chosen. The CQLF-based stability test, involving the LMIs formulated in (24)–(26) shows that the individual closed-loop systems resulting from these two controllers possess a CQLF. As can be seen in Fig. 10, the comfort gain between the two chosen controllers is significant and for the considered road profile the controller $\mathbf{k}_{\text{comf}}^T$ does not violate the rms-limit [see (7) with $F_{\text{stat}}/3 \approx 387$ N] for the dynamic wheel load.

After $\mathbf{k}_{\text{comf}}^T$, $\mathbf{k}_{\text{safe}}^T$ and the matrix $\mathbf{P}$ of the CQLF have been fixed, the suspension deflection controller $\mathbf{k}_{\text{susp}}^T$ is designed such that (24) is satisfied with the matrices $\mathbf{A}^{(5)}$, $\mathbf{A}^{(6)}$ given in (27). To this end, the weighting term $q_{x_{cw}}$ in (32) of the safety-oriented controller $\mathbf{k}_{\text{safe}}^T$ is successively increased and for every increase the condition (24) for the CQLF is tested with $\mathbf{A}^{(5)}$, $\mathbf{A}^{(6)}$. The suspension controller parametrization results from this iterative procedure from the weight vector η with the highest value of $q_{x_{\text{cw}}}$, for which (24) is still satisfied with $\mathbf{A}^{(5)}$, $\mathbf{A}^{(6)}$. The rationale behind this procedure is the fact that driving states, which are critical for the dynamic wheel load, are frequently also critical for suspension deflection. By this procedure, the suspension deflection weight has been increased from $q_{x_{\text{cw}}}^{\text{safe}} = 1.5849 \cdot 10^{10}$ to $q_{x_{\text{cw}}}^{\text{susp}} = 3.5413 \cdot 10^{10}$.

[3] It is noted that this model is controllable and observable.

[4] This is without loss of generality since the state feedback gain, which minimizes the cost functional (31) with $\mathbf{Q}_y$ and $R = 1$, also minimizes the cost functional with $c\mathbf{Q}_y$ and $R = c$ for any $c > 0$.

The numerical values for the three suspension controllers and the matrix $\mathbf{P}$ of the derived CQLF (rounded to multiples of 10^{-2} and 10^{-4}, respectively) are

$$\mathbf{k}_{\text{comf}}^T = \begin{bmatrix} -7605.45 & 21.25 & 789.35 & 364.00 \end{bmatrix} \quad (36)$$

$$\mathbf{k}_{\text{safe}}^T = \begin{bmatrix} -7626.72 & 42.00 & -20578.39 & -503.75 \end{bmatrix} \quad (37)$$

$$\mathbf{k}_{\text{susp}}^T = \begin{bmatrix} -7245.52 & 132.82 & -20923.90 & -500.93 \end{bmatrix} \quad (38)$$

$$\mathbf{P} = \begin{bmatrix} 5.5024 & 0.8632 & -5.2069 & 0.0128 \\ 0.8632 & 0.8574 & -4.2785 & 0.0121 \\ -5.2069 & -4.2785 & 2060.9480 & 0.2039 \\ 0.0128 & 0.0121 & 0.2039 & 0.3257 \end{bmatrix}. \quad (39)$$

In the proposed controller design approach, the CQLF-based stability test, involving the LMIs formulated in (24)–(27) is performed after the Pareto front, which shows the controller performance, has been generated. Although this might be considered as a drawback of the proposed approach from a control theoretical point of view, it increases the transparency of the achievable controller performance, which is determined using the nonlinear model of the suspension for the controller optimization. By the proposed optimization approach, the suspension designer gets a clear sense of the performance achievable with the controllers for the nonlinear model and can then pick a set of controllers based on their performance and the desired suspension characteristic of the vehicle. Afterwards it is checked for $\mathbf{k}_{\text{comf}}^T$ and $\mathbf{k}_{\text{safe}}^T$ if the stability conditions (24)–(26) are satisfied. If the conditions were not satisfied, it would be an iterative procedure choosing a different set of controllers, which are located "closer to each other" on the Pareto front, thus offering a slightly lower performance until a set of controllers is found that satisfies (24)–(26). Afterwards the suspension deflection controller $\mathbf{k}_{\text{susp}}^T$ is designed employing the abovementioned procedure that involves the test if (27) is also satisfied for the resulting set of three controllers.

D. Interpolation Performance

The proposed interpolation approach (17) offers continuous control signals and involves only a small number of state feedback controllers to be stored in an electronic control unit. The stability of the approach has been studied in the last Section. In the following, it is analyzed which performance results from the interpolation-based control law (17) and if the number of $N = 3$ controllers is sufficient.

An important fact is that the state feedback gain resulting from the interpolation of the LQRs formulated in (17) is in general not an LQR in terms of the quadratic cost functional (33). However, if the resulting performance is comparable to the LQR performance given by the Pareto front in Fig. 10 and the suspension deflection does not rise significantly, the interpolation method is suitable for the adaptive suspension control approach. To verify the performance of the controller parametrizations resulting from the interpolation, the co-domains of $q_{\text{fdyn}}(t)$ and $q_{\text{susp}}(t)$ have been quantized and simulations with the nonlinear test rig model have been performed for the resulting controller configurations using profile P1 as excitation ($v_{p1} = 50$ km/h). In order to study the performance with respect to the system requirements

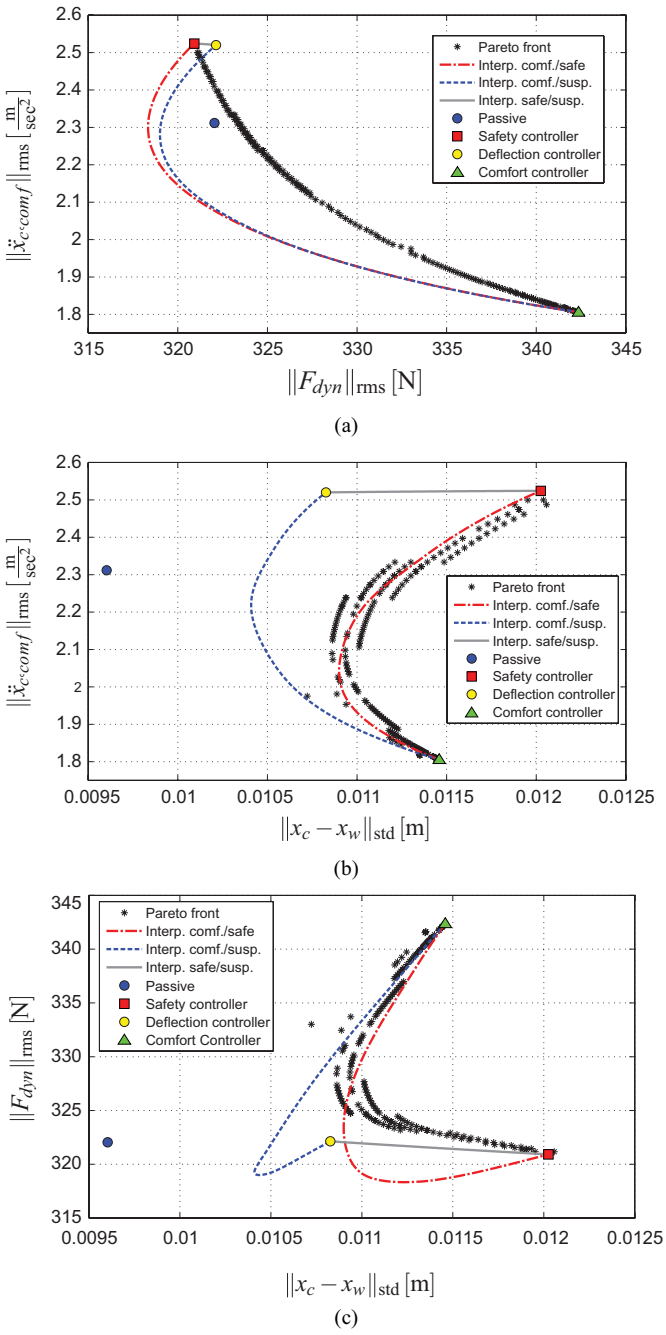

Fig. 11. Performance results for the interpolation between the controllers $\mathbf{k}_{\text{comf}}^T$, $\mathbf{k}_{\text{safe}}^T$, and $\mathbf{k}_{\text{susp}}^T$ in comparison to the LQR configurations of the Pareto front of Fig. 10. (a) Ride comfort versus ride safety. (b) Ride comfort versus suspension deflection. (c) Ride safety versus suspension deflection.

described in Section II-C, the carpet plots resulting from the interpolation between each pair of controllers are depicted for the quantities $\|\ddot{x}_{c,\text{comf}}\|_{\text{rms}}$, $\|F_{\text{dyn}}\|_{\text{rms}}$ and $\|x_c - x_w\|_{\text{std}}$ in Fig. 11. Note that due to the more transparent representation only the resulting performance from interpolating between two controllers is depicted in each case. However, further simulations have shown that the depicted performance regions in the conflict diagrams are representative bounds for the performance resulting for controller parametrizations with $0 < q_{\text{fdyn}} < 1 \wedge 0 < q_{\text{susp}} < 1$. The Pareto front from Fig. 10 and the passive suspension configuration are also shown in each conflict diagram.

As Fig. 11 shows, the performance of the interpolated state feedback gains is even better with respect to most aspects than the performance of the LQRs from the Pareto front. The suspension deflection controller offers significant benefit in terms of $\|x_c - x_w\|_{\text{std}}$ [Fig. 11(b)], while it only marginally deteriorates ride comfort and ride safety [Fig. 11(a)]. None of the controllers resulting from the interpolation violates the bounds on the dynamic wheel load ($\|F_{\text{dyn}}\|_{\text{rms}} \leq 387\,\text{N}$ and $\min(F_{\text{dyn}}) > -1160.5\,\text{N}$) or the suspension deflection ($\|x_c - x_w\|_{\text{std}} \leq 1.67\,\text{cm}$ and $\max(|x_c - x_w|) \leq 5\,\text{cm}$). Although it becomes apparent that the LQR approach does not achieve the optimal overall performance for the considered realistic suspension setting, no controller parametrization results from the considered interpolation approach, which dominates the comfort controller in terms of ride comfort. Since the interpolation-based adaptive controller outperforms the LQR configurations regarding ride safety and suspension deflection, it represents a feasible approach, which offers a fairly transparent controller design process and a significant performance potential.

V. Experimental Validation

The experiments to validate the performance capability of the proposed adaptive control approach are conducted on the test rig presented in Section II-A. To provide a realistic framework, the two real measured road profiles (being passed with $v_{p1} = 50$ km/h and $v_{p2} = 30$ km/h, respectively) as well as the synthetic singular disturbance event (with $\hat{h} = 4.5\,\text{cm}$, $L = 0.5\,\text{m}$, $v_b = 8$ km/h), which have been described in Section II-B, are used as excitation signals.

A. Benchmark Systems

For the evaluation of the performance of the proposed control approach, the following benchmark systems are utilized besides the passive suspension system.

1) *Skyhook Controller:* In this established suspension control concept (proposed for semi-active dampers by Karnopp in [9]), a skyhook damping force $\tilde{F}_{\text{d,sky}} = -d_{\text{sky}}\dot{x}_c$ is generated to reduce the absolute velocity $\dot{x}_c$ of the chassis mass. The skyhook controller is employed for the active suspension configuration (Act.-Skyh.) and an emulation of a semi-active suspension (SA-Skyh.). For the implementation, a lower passive damping ratio ($\tilde{D}_{c,p} = 0.28$ resembling a linear damper with $d_c = 500$ Nsec/m) is emulated by the actuator before the skyhook damping force (with $d_{\text{sky}} = 2000$ Nsec/m) is superimposed since the original damper characteristic of the ATV provides a more safety-oriented suspension configuration and the skyhook damping could not achieve significant comfort gain in the semi-active case. Both damping coefficients d_c and d_{sky} have been determined by conflict diagram-based optimization in a similar manner as the controller parametrization described in Section IV-C. The resulting damping force in the suspension is

$$\tilde{F}_d = -d_{\text{sky}}\dot{x}_c - d_c(\dot{x}_c - \dot{x}_w). \tag{40}$$

In the semi-active case, the actuator control logic clips the skyhook control force if it violates the passivity restriction $\tilde{F}_d(t)\,(\dot{x}_c(t) - \dot{x}_w(t)) \leq 0$.

2) *Adaptive Skyhook Controller:* The adaptation logic presented in Section IV-A is used to interpolate between two semi-active controller settings according to the current driving state. The first setting is the comfort-oriented skyhook setting described above. The second setting is more safety oriented with $d_c = 500$ Nsec/m and $d_{\text{sky}} = 0$ Nsec/m. The adaptive skyhook controller (SA-Ad.) is implemented for the emulated semi-active suspension configuration.
3) *Classical LQR:* From the Pareto front depicted in Fig. 10, a moderately tuned comfort-oriented LQR is chosen that exhibits a dynamic wheel load exactly between the passive configuration and the comfort controller, i.e., $\|F_{\text{dyn}}\|_{\text{rms}} = 331\,\text{N}$.

B. Performance Evaluation

Based on the system requirements formulated in Section II-C, performance measures are derived. In this context, the suspension performance of each analyzed controller configuration relative to the passive suspension system is of particular interest. Consequently, the performance gain

$$P_{g,\text{obj}} = 1 - \frac{\|\text{obj}_{\text{cont}}\|_i}{\|\text{obj}_{\text{pass}}\|_i} \tag{41}$$

is introduced, where $\|\text{obj}_{\text{cont}}\|_i$ denotes the absolute performance of the controlled suspension with respect to any of the given criteria $\|\cdot\|_i$ (rms-value, peak values etc.) and $\|\text{obj}_{\text{pass}}\|_i$ is the performance of the passive reference. A positive value of $P_{g,\text{obj}}$ denotes a reduction of the absolute value of the corresponding quantity and thus a performance improvement.

C. Measurement Results

Fig. 12 shows the measurement signals for the singular disturbance event. The fast adaptation prevents the limits for the dynamic wheel load and the suspension deflection to be exceeded and the peaks in the vertical chassis acceleration are lowered so that a performance gain of $P_{g,\|\ddot{x}_{c,comf}\|_{\text{rms}}} \approx 35\%$ with respect to the passive suspension can be achieved. The resulting performance gains [see (41)] are summarized in the spider charts in Fig. 13 for all three considered excitation signals[5] (in the diagrams, the center represents $P_{g,\text{obj}} \leq -40\%$). In terms of suspension deflection, the peak deflection in compression direction ($\min(x_c - x_w)$) of the suspension strut is analyzed since hitting the compression endstop is particularly critical in terms of ride comfort and wear of components.

The semi-active skyhook controllers (SA-Skyh. and SA-Ad.) can only slightly enhance ride comfort although the adaptive skyhook approach offers advantages regarding peak chassis acceleration over the conventional skyhook controller for P1. Especially for profile P2, which primarily contains high frequency components being critical for ride safety despite

[5]The interested reader can find plots of the corresponding measurement signals for profile P1 in [35].

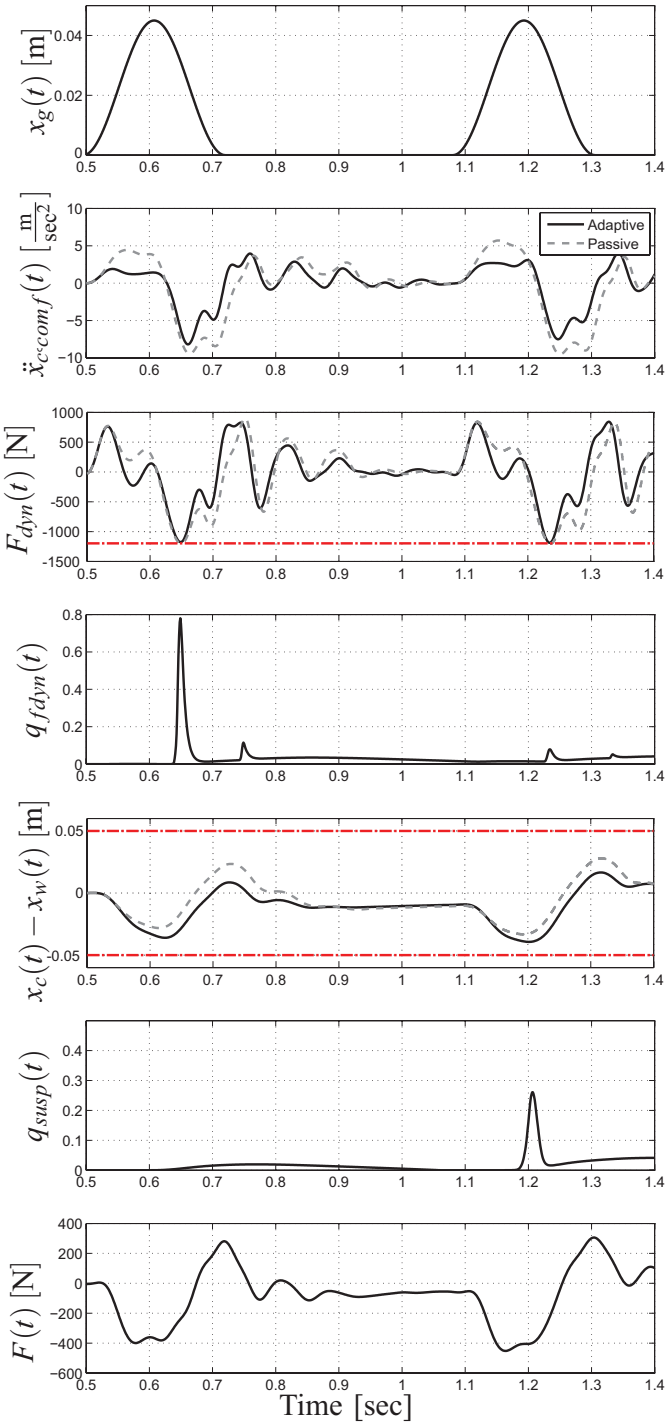

Fig. 12. Measurement results of the adaptively controlled suspension versus the passive suspension (singular disturbance event); the dashed-dotted lines indicate the limits for the peak-value of F_{dyn} (i.e., $-F_{\text{stat}}$) and the suspension deflection limits.

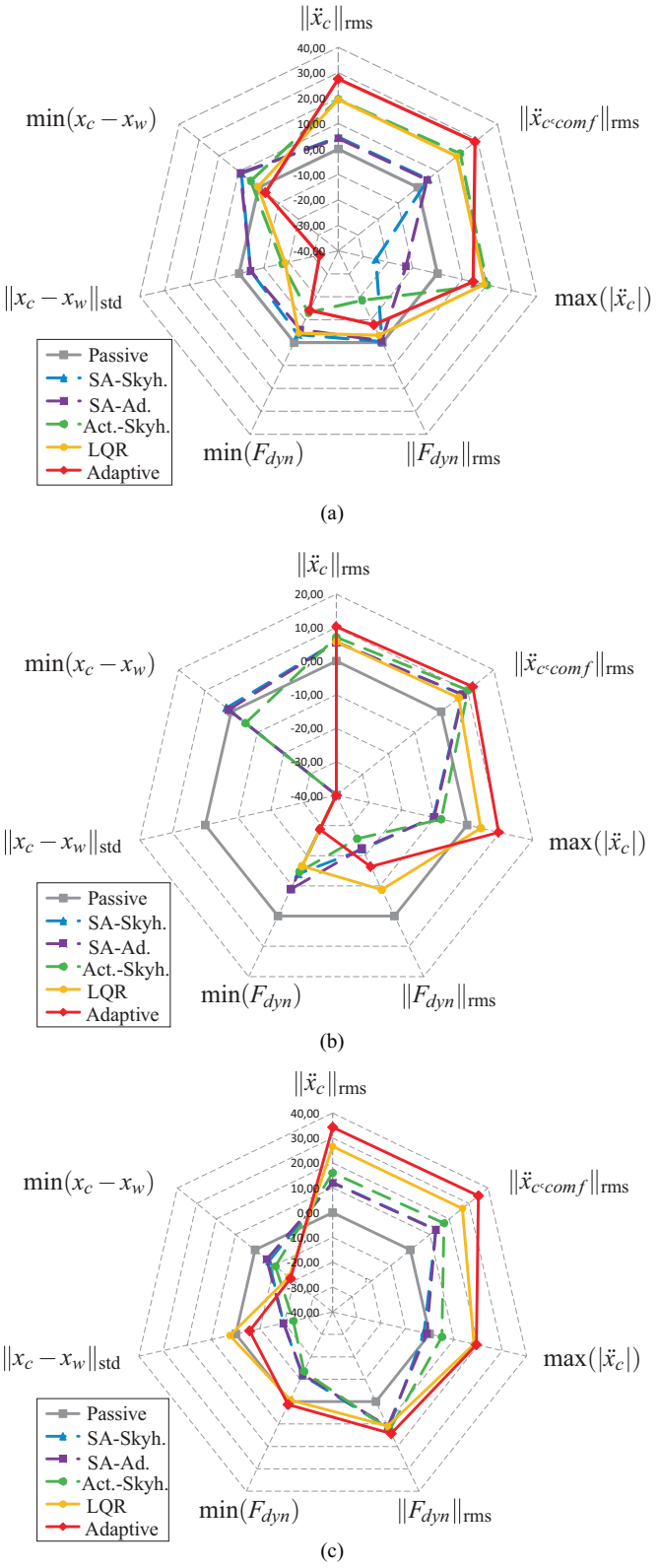

Fig. 13. Measurement results of the controller performance for (a) profile P1 with $v_{p1} = 50$ km/h, (b) profile P2 with $v_{p2} = 30$ km/h, and (c) singular disturbance event.

their low amplitudes, the absolute velocity of the chassis mass is too low to benefit from skyhook damping. The performance deterioration in terms of suspension deflection is uncritical for all controllers for profile P2 since the passive reference shows very low suspension deflections for this road profile ($\|x_c - x_w\|_{\text{std}} = 0.25\,\text{cm}$ and $\min(x_c - x_w) = -1.1\,\text{cm}$). The active skyhook controller (Act.-Skyh.) in comparison achieves significantly better ride comfort for P1, which comes at the price of violating the rms-limit of the dynamic wheel load and the highest power consumption of all considered active suspension configurations ($\|P^+\|_{\text{rms}} = 46.9$ W for P1). Unlike the active skyhook controller, the LQR and the

adaptive controller can increase ride comfort for P2 and the singular disturbance event while keeping the dynamic wheel load peaks at levels of the passive suspension system for the latter excitation profile. An important fact for the performance in terms of the dynamic wheel load is that the passive system, which is the reference for the calculation of the performance gain in (41), has a very ride safety-oriented suspension design due to a comparably high passive damping (damping ratio of the unsprung mass $D_c \approx 0.39$). Thus, increases in the dynamic wheel load do not immediately effect ride safety in a critical way as long as the given bound (7) for the dynamic wheel load is not violated.

The LQR performs well for all considered excitation signals (power consumption $\|P^+\|_{\text{rms}} = 17\,\text{W}$ for P1). The adaptive controller, however, offers by far the best ride comfort for all considered road profiles while keeping the constraints for the suspension deflection and the dynamic wheel load formulated in Section II-C. Its power consumption for P1 ($\|P^+\|_{\text{rms}} = 24.8\,\text{W}$) is lower than the one of the active skyhook controller (Act.-Skyh.).

The performance advantage of the adaptive controller becomes even more apparent if the amplitude of profile P1 is increased by 25%. The adaptive controller can improve ride comfort even by 31.41% and still keeps the rms-limit for the dynamic wheel load as well as the suspension deflection limit while all considered benchmark systems, including the passive system violate the dynamic wheel load and/or the suspension deflection limits.

VI. Conclusion

In this paper it has been experimentally shown that the proposed adaptive control approach can overcome the conservatism, which is frequently introduced by time-invariant suspension controllers. Moreover, a framework was presented to ensure stability of the adaptively controlled suspension. The proposed controller structure offers significant ride comfort improvements while keeping the limits on suspension deflection and dynamic wheel load for all considered realistic excitation profiles. The proposed adaptive controller outperformed the considered benchmark controllers, which partially (LQR and fast adaptive skyhook concept) even go beyond the state-of-the-art of suspension controllers integrated in production vehicles. The objective in this paper is the maximization of ride comfort. However, the modular controller structure could also be adjusted to rather focus on vehicle handling improvements by minimizing the dynamic wheel load. According adjustments in the adaption logic can be made without affecting the stability of the system. In order to utilize the performance potential of the proposed control approach in modern efficiency focused production vehicles, future work will involve the further development of driving state adaptive control strategies for semi-active suspension configurations.

Acknowledgment

The authors would like to thank B. Lohmann, M. Buhl, and N. Pletschen for fruitful discussions and helpful hints as well as support with the layout of this paper.

References

[1] M. Mitschke and H. Wallentowitz, *Dynamik der Kraftfahrzeuge*. Berlin, Germany: Springer-Verlag, 2004.
[2] D. Hrovat, "Survey of advanced suspension developments and related optimal control applications," *Automatica*, vol. 33, no. 10, pp. 1781–1817, 1997.
[3] S. M. Savaresi, C. Poussot-Vassal, C. Spelta, O. Sename, and L. Dugard, *Semi-Active Suspension Control Design for Vehicles*. London, U.K.: Butterworth, 2010.
[4] *Mechanical Vibration and Shock—Evaluation of Human Exposure to Whole-Body Vibration*, ISO Standard 2631-1:1997, 1997.
[5] R. S. Sharp and D. A. Crolla, "Road vehicle system design—a review," *Veh. Syst. Dynamics*, vol. 16, no. 3, pp. 167–192, 1987.
[6] D. Fischer and R. Isermann, "Mechatronic semi-active and active vehicle suspensions," *Control Eng. Pract.*, vol. 12, no. 11, pp. 1353–1367, 2004.
[7] D. Karnopp, "Theoretical limitations in active vehicle suspensions," *Veh. Syst. Dynamics*, vol. 15, no. 1, pp. 41–54, 1986.
[8] J. K. Hedrick and T. Butsuen, "Invariant properties of automotive suspensions," *Proc. Inst. Mech. Eng., D, J. Automobile Eng.*, vol. 240, no. 14, pp. 21–27, 1990.
[9] D. Karnopp, M. J. Crosby, and R. A. Harwood, "Vibration control using semi-active force generators," *ASME J. Eng. Ind.*, vol. 96, no. 2, pp. 619–626, 1974.
[10] S. Savaresi and C. Spelta, "Mixed sky-hook and ADD: Approaching the filtering limits of a semi-active suspension," *ASME Trans., J. Dynamic Syst., Meas. Control*, vol. 129, no. 4, pp. 382–392, 2007.
[11] S. Savaresi and C. Spelta, "A single-sensor control strategy for semi-active suspensions," *IEEE Trans. Control Syst. Technol.*, vol. 17, no. 1, pp. 143–152, Jan. 2009.
[12] R. K. Mehra, J. N. Amin, K. J. Hedrick, C. Osorio, and A. Gopalasany, "Active suspension using preview information and model predictive control," in *Proc. IEEE Int. Conf. Control Appl.*, Oct. 1997, pp. 860–865.
[13] A. Akbari, "Multi-objective H_∞/GH_2 preview control of active vehicle suspensions," Ph.D. dissertation, Inst. Automatic Control, Faculty Mech. Eng., TU München, München, Germany, 2009.
[14] S. Savaresi, E. Silani, and S. Bittanti, "Acceleration driven damper (ADD): An optimal control algorithm for comfort oriented semi-active suspensions," *ASME Trans., J. Dyn. Syst., Meas. Control*, vol. 127, no. 2, pp. 218–229, 2005.
[15] T. Kloiber, G. Koch, and B. Lohmann, "Modified optimal control of a nonlinear active suspension system," in *Proc. 49th IEEE Conf. Decision Control*, Dec. 2010, pp. 5572–5577.
[16] C. Lauwerys, J. Swevers, and P. Sas, "Robust linear control of an active suspension on a quarter car test-rig," *Control Eng. Pract.*, vol. 13, no. 5, pp. 577–586, 2005.
[17] A. Zin, O. Sename, P. Gaspar, L. Dugard, and J. Bokor, "Robust LPV-$\mathcal{H}_\infty$ control for active suspensions with performance adaptation in view of global chassis control," *Veh. Syst. Dynamics*, vol. 46, no. 10, pp. 889–912, 2008.
[18] M. Canale, M. Milanese, and C. Novara, "Semi-active suspension control using 'fast' model-predictive techniques," *IEEE Trans. Control Syst. Technol.*, vol. 14, no. 6, pp. 1034–1046, Nov. 2006.
[19] Y. Zhang and A. Alleyne, "A practical and effective approach to active suspension control," *Veh. Syst. Dynamics*, vol. 43, no. 5, pp. 305–330, 2005.
[20] L. Zuo, J.-J. E. Slotine, and S. A. Nayfeh, "Model reaching adaptive control for vibration isolation," *IEEE Trans. Control Syst. Technol.*, vol. 13, no. 4, pp. 611–617, Jul. 2005.
[21] M. Ramsbottom and D. A. Crolla, "Simulation of an adaptive controller for a limited-bandwidth active suspension," *Int. J. Veh. Design*, vol. 21, nos. 4–5, pp. 355–371, 1999.
[22] A. Alleyne and J. K. Hedrick, "Nonlinear adaptive control of active suspensions," *IEEE Trans. Control Syst. Technol.*, vol. 3, no. 1, pp. 94–101, Mar. 1995.
[23] R. S. Sharp and S. A. Hassan, "On the performance capabilities of active automobile suspension systems of limited bandwidth," *Veh. Syst. Dynamics*, vol. 16, no. 4, pp. 213–225, 1987.
[24] D. Karnopp and D. Margolis, "Adaptive suspension concepts for road vehicles," *Veh. Syst. Dynamics*, vol. 13, no. 3, pp. 145–160, 1984.
[25] A. Hać, "Adaptive control of vehicle suspensions," *Veh. Syst. Dynamics*, vol. 16, no. 2, pp. 57–74, 1987.
[26] P. J. T. Venhovens, "Optimal control of vehicle suspensions," Ph.D. dissertation, Faculty Mechanical Eng. & Marine Technol., Delft Univ. Technol., Delft, The Netherlands, 1993.
[27] J. Lin and I. Kanellakopoulos, "Road-adaptive nonlinear design of active suspensions," in *Proc. Amer. Control Conf.*, vol. 1. 1997, pp. 714–718.

[28] I. J. Fialho and G. J. Balas, "Road adaptive active suspension design using linear parameter-varying gain-scheduling," *IEEE Trans. Control Syst. Technol.*, vol. 10, no. 1, pp. 43–54, Jan. 2002.

[29] C. Poussot-Vassal, A. Drivet, O. Sename, L. Dugard, and R. Ramirez-Mendoza, "A self tuning suspension controller for multi-body quarter vehicle model," in *Proc. 17th IFAC World Congr.*, 2008, pp. 3410–3415.

[30] J. Lu, "A frequency-adaptive multi-objective suspension control strategy," *ASME J. Dynamic Syst., Meas., Control*, vol. 126, no. 3, pp. 700–707, 2004.

[31] C. Poussot-Vassal, O. Sename, L. Dugard, P. Gáspár, Z. Szabó, and J. Bokor, "Attitude and handling improvements through gain-scheduled suspensions and brakes control," *Control Eng. Pract.*, vol. 19, no. 3, pp. 252–263, 2011.

[32] K.-S. Hong, H.-C. Sohn, and J. K. Hedrick, "Modified skyhook control of semi-active suspensions: A new model, gain scheduling, and hardware-in-the-loop tuning," *J. Dynamic Syst., Meas., Control*, vol. 124, no. 1, pp. 158–167, 2002.

[33] K. Yi and B. S. Song, "A new adaptive sky-hook control of vehicle semi-active suspensions," *Proc. Inst. Mech. Eng., D, J. Automobile Eng.*, vol. 213, no. 3, pp. 293–303, 1999.

[34] G. Koch, K. J. Diepold, and B. Lohmann, "Multi-objective road adaptive control of an active suspension system," in *Motion and Vibration Control*, H. Ulbrich and L. Ginzinger, Eds. New York, USA: Springer-Verlag, 2008, pp. 189–200.

[35] G. Koch, "Adaptive control of mechatronic vehicle suspension systems," Ph.D. dissertation, Inst. Automatic Control, Faculty Mechanical Eng., TU München, München, Germany, 2011.

[36] G. Koch, E. Pellegrini, S. Spirk, and B. Lohmann, "Design and modeling of a quarter-vehicle test rig for active suspension control," Inst. Autom. Control, TU München, München, Germany, Tech. Rep. TRAC-5(2), Jul. 2010.

[37] *VDI Guideline 2057—Human Exposure to Mechanical Vibrations*, Verein Deutscher Ingenieure, München, Germany, Sep. 2002.

[38] W. Matschinsky, *Radführungen der Straßenfahrzeuge - Kinematic, Elasto-Kinematik und Konstruktion*. New York, USA: Springer-Verlag, 2007.

[39] H. Olsson, K. J. Åström, C. C. de Wit, M. Gäfvert, and P. Lischinsky, "Friction models and friction compensation," *Eur. J. Control*, vol. 4, no. 3, pp. 176–195, 1998.

[40] U. Kramer, *Kraftfahrzeugführung: Modelle, Simulation und Regelung*. New York, USA: Springer-Verlag, 2007.

[41] J. Lunze, *Automatic Control 1 (in German)*. Berlin, Germany: Springer-Verlag, 2001.

[42] G. Koch, O. Fritsch, and B. Lohmann, "Potential of low bandwidth active suspension control with continuously variable damper," *Control Eng. Pract.*, vol. 18, no. 11, pp. 1251–1262, 2010.

[43] G. Koch, T. Kloiber, E. Pellegrini, and B. Lohmann, "A nonlinear estimator concept for active vehicle suspension control," in *Proc. Amer. Control Conf.*, 2010, pp. 4576–4581.

[44] S. Ohsaku, "Vorrichtung und Verfahren zum Schätzen einer kinetischen Zustandsgröße für Kraftfahrzeuge," D.E. Patent 10016898, Sep. 2, 2010.

[45] G. Koch, T. Kloiber, and B. Lohmann, "Nonlinear and filter based estimation for vehicle suspension control," in *Proc. 49th IEEE Conf. Decision Control*, Dec. 2010, pp. 5592–5597.

[46] B. Heißing, *Fahrwerkhandbuch*, M. Ersoy, Ed. Wiesbaden, Germany: Vieweg Verlag, 2007.

[47] H. K. Khalil, *Nonlinear Systems*, 2nd ed. Englewood Cliffs, NJ, USA: Prentice-Hall, 1996.

[48] Z. Geng and L. Huang, "Robust stability of the systems with mixed uncertainties under the IQC descriptions," *Int. J. Control*, vol. 73, no. 9, pp. 776–786, 2000.

[49] J. Löfberg, "Yalmip : A toolbox for modeling and optimization in MATLAB," in *Proc. Comput. Aided Control Syst. Design Conf.*, Sep. 2004, pp. 284–289.

[50] J. F. Sturm, "Using SeDuMi 1.02, a Matlab toolbox for optimization over symmetric cones," *Optim. Methods Softw.*, vol. 11, nos. 1–4, pp. 625–653, 1999.

[51] J. J. E. Slotine and W. Li, *Applied Nonlinear Control*. Englewood Cliffs, NJ, USA: Prentice-Hall, 1991.

[52] K. Deb, A. Pratap, S. Agarwal, and T. Meyarivan, "A fast and elitist multiobjective genetic algorithm: NSGA-II," *IEEE Trans. Evol. Comput.*, vol. 6, no. 2, pp. 182–197, Apr. 2002.

[53] E. Alfaro-Cid, E. McGookin, and D. Murray-Smith, "Optimisation of the weighting functions of an H_∞ controller using genetic algorithms and structured genetic algorithms," *Int. J. Syst. Sci.*, vol. 39, no. 4, pp. 335–347, 2008.

Guido Koch received the Bachelor's degree in general engineering science and the Master's degree in mechatronics from the Hamburg University of Technology, Hamburg, Germany, in 2004 and 2005, respectively, and the Ph.D. degree in mechanical engineering from the Technische Universität München, Munich, Germany, in 2011.

He was a Researcher with the Institute of Automatic Control, Technische Universität München, until 2011, where he focused on automotive suspension control and active vibration control. From 2011 to 2012, he was a Post-Doctoral Research Fellow with the Dynamic Design Laboratory, Stanford University, Stanford, CA, USA, where he was involved in research on vehicle control at the limits of handling and autonomous vehicles. Since 2012, he has been working for a global management consulting firm.

Tobias Kloiber received the Dipl.-Ing. degree in mechanical engineering from the Technische Universität München, Munich, Germany, in 2010, where he is currently pursuing the Ph.D. (Dr.-Ing.) degree with the Institute of Automatic Control.

He is currently a Researcher with the Institute of Automatic Control, Technische Universität München. His current research interests include nonlinear control, passivity-based control, switched systems, and active vibration control.